Neuro-Oncology Advances

1(1), 1–11, 2019 | doi:10.1093/noajnl/vdz012 | Advance Access date 2 July 2019

A comprehensive preclinical assessment of late-term imaging markers of radiation-induced brain injury

Tien T. Tang†, Janice A. Zawaski†, Shelli R. Kesler, Christine A. Beamish, Wilburn E. Reddick, John O. Glass, Darrell H. Carney, Omaima M. Sabek, David R. Grosshans, and M. Waleed Gaber

Department of Pediatrics, Hematology-Oncology Section, Dan L. Duncan Comprehensive Cancer Center, Baylor College of Medicine, Houston, Texas (T.T.T., J.A.Z., M.W.G.); Department of Neuro-Oncology, The University of Texas MD Anderson Cancer Center, Houston, Texas (S.R.K.); Department of Surgery, Houston Methodist Research Institute, Houston, Texas (C.A.B., O.M.S.); Department of Diagnostic Imaging, St. Jude Children's Research Hospital, Memphis, Tennessee (W.E.R., J.O.G.); Department of Biochemistry and Molecular Biology, The University of Texas Medical Branch, Galveston, Texas and Chrysalis BioTherapeutics, Inc., Galveston, Texas (D.H.C.); Department of Molecular Physiology and Biophysics, Baylor College of Medicine, Houston, Texas (M.W.G.); Departments of Radiation and Experimental Radiation Oncology, The University of Texas MD Anderson Cancer Center, Houston, Texas (D.R.G.); Department of Bioengineering, Rice University, Houston, Texas (T.T.T., M.W.G.)

Corresponding Author: M. Waleed Gaber, PhD, Department of Pediatrics, Hematology-Oncology Section, Baylor College of Medicine, 1102 Bates Street, Suite 200.04, Houston, TX 77030, USA (gaber@bcm.edu).

†These authors contributed equally to this work.http://creativecommons.org/licenses/by-nc/4.0/

Abstract

Background. Cranial radiotherapy (CRT) is an important part of brain tumor treatment, and although highly effective, survivors suffer from long-term cognitive side effects. In this study we aim to establish late-term imaging markers of CRT-induced brain injury and identify functional markers indicative of cognitive performance. Specifically, we aim to identify changes in executive function, brain metabolism, and neuronal organization.

Methods. Male Sprague Dawley rats were fractionally irradiated at 28 days of age to a total dose of 30 Gy to establish a radiation-induced brain injury model. Animals were trained at 3 months after CRT using the 5-choice serial reaction time task. At 12 months after CRT, animals were evaluated for cognitive and imaging changes, which included positron emission tomography (PET) and magnetic resonance imaging (MRI).

Results. Cognitive deficit with signs of neuroinflammation were found at 12 months after CRT in irradiated animals. CRT resulted in significant volumetric changes in 38% of brain regions as well as overall decrease in brain volume and reduced gray matter volume. PET imaging showed higher brain glucose uptake in CRT animals. Using MRI, irradiated brains had an overall decrease in fractional anisotropy, lower global efficiency, increased transitivity, and altered regional connectivity. Cognitive measurements were found to be significantly correlated with six image features that included myelin integrity and local organization of the neural network.

Conclusions. These results demonstrate that CRT leads to late-term morphological changes, reorganization of neural connections, and metabolic dysfunction. The correlation between imaging markers and cognitive deficits can be used to assess late-term side effects of brain tumor treatment and evaluate efficacy of new interventions.

Key Points

1. Cranial irradiation induces late-term metabolic dysfunction and neuroinflammation.
2. Connectome reveals trends toward reorganization of the neural network after radiation.
3. Discovery of image features that may be indicative of cognitive performance.

© The Author(s) 2019. Published by Oxford University Press, the Society for Neuro-Oncology and the European Association of Neuro-Oncology.
This is an Open Access article distributed under the terms of the Creative Commons Attribution Non-Commercial License (http://creativecommons.org/licenses/by-nc/4.0/), which permits non-commercial re-use, distribution, and reproduction in any medium, provided the original work is properly cited. For commercial re-use, please contact journals.permissions@oup.com

Importance of the Study

Cranial radiotherapy is highly effective for tumor control however pediatric survivors often suffer from cognitive deficits. Currently, cognitive testing provides a readout of the underlying biological changes. However, there are no established markers for the risk assessment or identification of radiation-induced brain injury. Identification of noninvasive functional markers of damage could provide clinicians with a new tool to help determine the severity of cranial radiotherapy treatment side effects on a patient-to-patient basis and monitor long-term treatment efficacy. In this study, using a preclinical pediatric radiation-induced brain injury model, we identified several imaging markers of late-term radiation-induced damage using both structural and functional imaging. Further validation of our results may support the incorporation of medical imaging into the standard clinical workflow with the goal of providing additional information to clinicians, ultimately resulting in better informed treatment decisions and improved radiotherapy outcomes.

Brain tumors are the second most common childhood cancer with medulloblastoma being the most common. Standard of care for medulloblastoma tumors consists of surgical resection followed by cranial radiotherapy (CRT) and adjuvant chemotherapy achieving a 5-year survival of 70%.[1,2]Although CRT is highly effective in providing local tumor control, most survivors will experience acute and late-term side effects due to radiation-induced normal brain tissue damage attributed to the normal tissue being in the irradiation field. Radiation-induced brain injury can lead to microvascular network damage, demyelination, and an inflammatory response with activation of astrocytes and microglia.[3–5] Acute molecular and cellular changes such as neuroinflammation can lead to long-term side effects which may not fully manifest for months or years after treatment.[6–8] Although individual patient outcomes are variable, survivors of childhood brain cancer experience cognitive deficits which includes executive function, reduced processing speed, deficiencies in working memory and attention.[6,9]

Medical imaging techniques such as magnetic resonance (MR) and positron emission tomography (PET) imaging are widely available techniques that can be used to characterize radiation-induced metabolic, anatomical and functional changes in brain tissue. Diffusion tensor imaging (DTI), an MR technique, has been successfully used in the clinic to detect imaging changes related to cognitive deficits.[10,11] Fractional anisotropy (FA) values, reflecting isotropic diffusion, have been used as markers of inflammation and to determine the integrity of neuronal myelination in white matter, which can be correlative of cognitive performance.[12,13] DTI data can also be informative of the trajectory of white matter fibers in three-dimensional space using tractography. Using this technique, the brain network or connectome can be modeled to provide insight into the functional organization of the brain.[14] PET imaging with ^{18}F-flurodeoxy-glucose (^{18}F-FDG), a glucose analogue, is commonly used in the clinic for the detection and staging of cancers.[15,16] ^{18}F-FDG accumulates in tissues with high metabolic activity such as solid tumors. This radioisotope has also been shown to accumulate in sites with inflammation and can be used to localize and quantify neuroinflammation.[17–20] Using these imaging modalities, MR and PET, it is possible to assess the later-term radiation-induced damage to the brain.

Identification of noninvasive functional markers of damage could provide clinicians with a new tool to help determine the severity of cranial radiotherapy treatment side effects on a patient-to-patient basis and monitor treatment efficacy long-term. Therefore, the aim of this study was to identify imaging markers, using MR and PET imaging techniques that will provide further insight into late-term radiation-induced brain injury and are indicative of cognitive outcome. Young adolescent rats were irradiated and cognitive performance, specifically executive function, was evaluated using the 5-choice serial reaction time task (5-CSRTT) at 12 months after CRT, which is analogous to the Cambridge Neuropsychological Test Automated Battery (CANTAB) assessment for humans.[21] Imaging data were acquired to investigate radiation-induced structural, connective and inflammatory changes in the brain due to CRT. Established imaging markers were then correlated to cognitive performance.

Methods

Establishing Radiation-Induced Brain Injury Model

Experimental timeline can be found in Supplementary Figure 1. Twenty Male Sprague Dawley rats at 28 days of age were divided into two groups: Sham and CRT. Under anesthesia, CRT animals received fractionated irradiation 6 Gy × 5 days (30 Gy total) using a Rad Source 2000 X-ray irradiator (160 kVp, 25 mA, 128 cGy/min, Rad Source Technologies, Inc.) from behind the eyes to the back of the ears. The rest of the body was lead shielded. Sham animals were anesthetized but received no radiation. All animal experiments were approved by Baylor College of Medicine's Institutional Animal Care and Use Committee.

Cognitive Testing

Executive function was assessed using 5-CSRTT. Prior to training/testing animals (n = 20) were food restricted to maintain 85%–90% of their free-feeding weight to provide

incentive for participation. 5-CSRTT was completed with software and equipment from Noldus Information Technology and Med Associates. At 3 months after CRT, animals were trained using the 5-CSRTT, following the target criteria established by Bari et al.[22]; additional details about this task can be found in Supplementary Material.

At approximately 12 months after CRT, animals were tested for 5 days at their individual final stage achieved during training and the average stage reached by the Sham cohort during training for an additional 5 days. The following metrics were measured to determine the animal's cognitive performance: percent accuracy, percent correct, premature responses, and number of omission.

Immunohistochemistry

Upon completion of all imaging and cognitive testing, whole brains were excised, fixed in 10% formalin, coronally sectioned, and embedded in paraffin. Fluorescent immunostaining was performed using antibodies for tumor necrosis factor alpha (TNFα), myelin basic protein, GFAP, and IBA. Sections (n = 4–5/group) were imaged (×20, Nikon A1) and analyzed using ImageJ software (v.1.50i, National Institutes of Health) to yield semiquantitative immunohistochemistry data. All cells were counted manually per image per region by a blinded investigator, and quantified relative to total proportion by 4′,6-diamidino-2-phenylindole (DAPI) presence. Additional details can be found in Supplementary Material.

Imaging: Positron Emission Tomography

At approximately 12 months after CRT, animals (n = 10) were imaged with ^{18}F-FDG. All computed tomography (CT) and PET images were acquired on an Inveon scanner (Siemens AG). Prior to imaging, animals were fasted approximately 12 hours. One hour prior to scanning, each animal received 12.58 MBq (340 μCi) of ^{18}F-FDG (Cyclotope,) intravascularly. Animals were anesthetized with isoflurane and respiration monitored during imaging. CT scans were acquired, followed by a 30-minute PET scan, reconstructed using OSEM3D and registered to the CT scan for attenuation correction. Using the acquired CT scan, regions were segmented using Inveon Research Workspace (Siemens AG). Uptake of radioisotope was measured using the standardize uptake value (SUV) and max SUV normalized to animal's body weight.

Imaging: T_1-weighted/T_2-weighted/Proton Density Scans

After PET/CT imaging animals were imaged on a 9.4T Bruker Biospec MRI scanner (Bruker BioSpin). Animals were anesthetized with isoflurane and monitored during imaging to maintain normal breathing rates. A T_1-weighted, T_2-weighted, and proton density scan was acquired with axial slice orientation and 256 matrix size. White matter, which was calculated as percent of the intracranial volume, gray matter, and cerebral spinal fluid was analyzed using an automated hybrid neural network segmentation and classification as described by Reddick et al.[23]

Imaging: Diffusion Tensor Imaging

Animals (n = 10) were killed for *ex vivo* DTI MRI scans. Samples were prepared according to the method described by Tyszka et al.[24] Brains were imaged using 20 distinct gradient directions on a 9.4T Bruker Biospec MRI scanner (Bruker BioSpin). All DTI processing and connectome analyses were performed as described by Sahnoune et al.[25] Briefly, ROIEditor, DTI studio,[26,27] template maps from Duke Center for *In vivo* Microscopy,[28] DiffeoMap,[29] AIR algorithm,[30,31] and large deformation diffeomorphic metric mapping (LDDMM)[32] were used for alignment, segmentation, and calculation. DTI studio software (www.mristudio.org) was used to generate various volume maps and calculate the average FA value. Masked tensors were used for fiber tracking where cutoffs for fiber initiation and fiber continuation were set to FA values of 0.3/0.3 with a 70° angle cutoff. Total fiber number, average fiber length, and maximal fiber length were calculated. Alignment of the brains was done to template maps obtained from the Duke Center for In Vivo Microscopy.

Connectomes were constructed for each animal with N = 132 nodes, network degree of E = number of edges, and a network density of $D = E/[(N \times (N-1))/2]$ representing the fraction of present connections to all possible connections. The following connectome properties were calculated using graph theoretical analysis as implemented in Brain Connectivity Toolbox[33] to characterize global connectome effects: Mclust = Model Based Clustering, Trans = Transitivity, Assort = Assortativity, Eglob = Global Efficiency, Eloc = Local Efficiency, Mod = Modularity, PathL = Path Length, Lambda = Characteristic Path Length, Gamma = Normalized Clustering Coefficient, and Sigma = Small Worldness Index (Gamma/Lambda).[33–35] Using 100 null networks, Lambda is normalized by the mean path length and Gamma is normalized by mean clustering coefficient.[36] Data are presented as the area under curve across multiple densities or thresholds.

Statistics

Statistical analyses were conducted using Prism 7 (GraphPad Software, Inc.). Statistical significance was established using a two-tailed Student t test and corrected for multiple comparisons using the Holm–Sidak method when appropriate. With multiple group comparison a two-way analysis of variance test was performed with Bonferroni correction. Data are reported as mean ± standard deviation unless otherwise noted. Box-and-whisker plot: box extends from the 25th to 75th percentiles, median value marked by line and whiskers extend from min to max. Correlation analysis of imaging features and cognitive performance was performed using Pearson's correlation. P-value for Pearson's correlation coefficient uses the t-distribution. Connectome statistics were performed using permutation testing for global metrics and the network-based statistic for regional analysis; additional details can be found in Supplementary Material.[37] Significance was established at $P \leq .05$.

Results

Phenotypical Characterization

Brain growth was stunted early on and persisted to 12 months after CRT. At 3 months after CRT, Sham brains were significantly larger than CRT (P = .011). Although Sham brains showed growth from 3 to 12 months (though not statistically significant), CRT brains did not grow and remained significantly smaller than Sham (P = .001) (Fig. 1A). Sham brains were significantly longer, as measured from olfactory bulb to the back of the cerebellum, but not wider than CRT brains demonstrating stunting in the rostral to caudal direction at 3 months (length/width ratio: P = .0048) and 12 months (length/width ratio: P = .0037) after CRT (Fig. 1B).

CRT induced a heterogeneous volumetric response within the brain. Volumetric analysis of specific brain regions, normalized to whole brain volume to account for differences in brain volume, showed that 8 of the 26 brain regions analyzed were significantly smaller in CRT brains than Sham (Supplementary Figure 2, Supplementary Table 1). The cerebellum and diagonal domain were the only regions showing volume increase after CRT (P = .013). The affected brain regions were not found to be localized to any specific area of the brain.

Assessment of Cognitive Performance

Cognitive performance, specifically executive function, was assessed using the 5-CSRTT with training beginning at approximately 3 months after CRT. At the end of training, the final stage achieved by Sham animals (Stage 7) was significantly higher compared to CRT (Stage 5, P = .0004) with most failing to complete Stage 5 (Supplementary Figure 3). Further analysis of the number of days spent in each stage found no significant differences between Sham and CRT animals between Stages 1 and 4, CRT animals however spent significantly more time in Stage 5 compared to Sham ($P \leq .0001$) (Supplementary Figure 3). These results confirm that a radiation-induced brain injury model was established that exhibits cognitive deficits.

At 12 months after CRT, animals' cognitive performance was assessed again with 5-CSRTT. When animals were tested at their corresponding individual stage achieved during training, there was no significant difference between Sham and CRT for percent accuracy, percent correct, omission, or premature responses. These results suggest that animals were able to remember the task and did not exhibit further cognitive decline. Daily breakdown and average, more than 5 days of testing, of each cognitive metric evaluated at individual stage achieved can be found in Supplementary Figure 4.

When tested at Stage 7, the average stage Sham group achieved during training, there were no significant differences between Sham and CRT animals in percent accuracy and premature responses (Fig. 2B and C). However, CRT animals did not achieve the same performance as Shams in percent correct (P = .005) and omission responses (P = .025) (Fig. 2A and D). These results showed that CRT animals were able to accurately perform the task with the same accuracy as Sham but did not have the same level of participation. Daily breakdown of each cognitive metric evaluated at Stage 7 can be found in Supplementary Figure 5.

Molecular Characterization of Late-Term CRT

Brain sections immunostained at 12 months after CRT showed several molecular changes. Analysis of the corpus callosum showed a significant reduction in myelin (P = .024) in CRT animals compared to Sham animals (Fig. 3A and B). We observed clear signs of inflammation in CRT brains with significantly higher number of cells expressing TNFα (P = .004) and a higher number of astrocytes (GFAP) expressing TNFα (P = .014) (Fig. 3C and D). However, there were no significant differences in the number of astrocytes between Sham and CRT animals. In the corpus callosum of CRT animals there were increased numbers of microglia (P = .05) as well as an increased numbers of microglia that expressed TNFα (P = .032) (Fig. 3E and F). These results

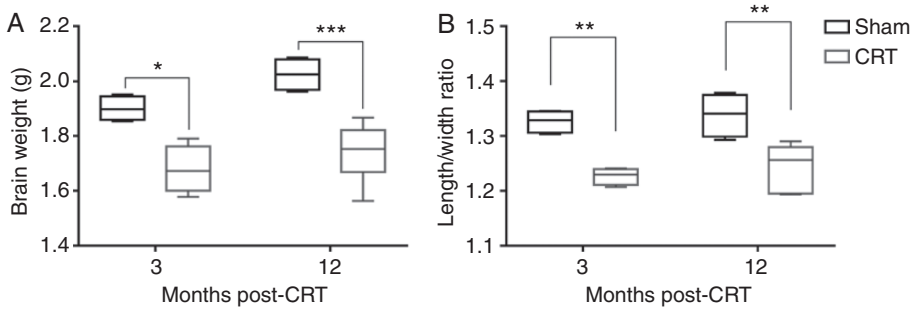

Fig. 1. Cranial radiotherapy (CRT) stunts brain growth. (**A**) Brain weight was measured at 3 and 12 months after CRT. Differences in brain weight were observed early and persist up to 12 months after CRT with limited growth in CRT brains. (**B**) Brain dimensions were measured at 3 and 12 months after CRT. CRT brains were significantly shorter while the width of the brain is preserved with no significant changes over time. *$P \leq .05$, **$P \leq .01$, ***$P \leq .001$.

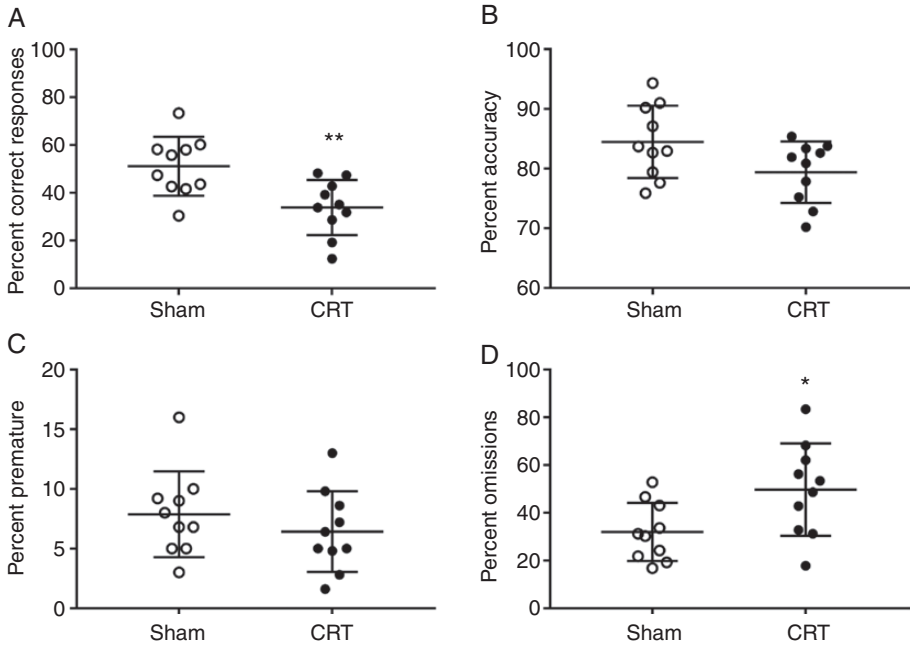

Fig. 2. Twelve months result of 5-choice serial reaction time task results at Stage 7. Cognitive performance was measured at Stage 7. (**A**) Correct response, (**B**) accuracy, (**C**) premature response, and (**D**) omission were averaged over the 5-day testing period. CRT animals had poor cognitive performance showing significantly lower correct response and higher omissions compared to Sham animals.*$P \leq .05$, **$P \leq .01$.

seem to indicate that there are late-term low levels of inflammation.

Metabolic activity of the brain was assessed using PET imaging at 12 months after CRT. Analysis of ^{18}FDG-PET data, with SUV normalized to body weight, showed significantly increased glucose uptake at 12 months after CRT (P = .005) throughout the brain (Fig. 4, Supplementary Table 2). Analysis of the max SUV, which is independent of the volume selected, further confirmed higher metabolic activity in CRT brains (P < .001) (Fig. 4).

Functional Changes of Late-Term CRT

DTI data at 12 months after CRT showed a significant decrease in whole brain FA value, which was observed in both white matter regions such as the fimbria and corpus callosum as well as in the isocortex, part of the cerebral cortex, gray matter region. The septum was the only region that showed a, significant increase in FA value in CRT animals compared to Sham (P = .048) (Fig. 5A). These FA changes indicate an overall change in myelin integrity after CRT. However, changes in FA values were not uniform across all brain regions with some regions showing more significant changes than others. FA values of individual brain regions can be found in Supplementary Table 3.

Fiber number was significantly reduced in CRT brains (P = .037), whereas average fiber length was significantly longer (P = .007) (Fig. 5B and C). There was no significant difference in the maximum fiber length. These results indicate that specific brain regions are more sensitive to radiation damage leading to deterioration of fiber tracts and myelin integrity which results in differences in overall fiber lengths, fiber number and FA values.

Network connectome analysis showed changes in global measures, which included lower global efficiency (Eglob, P = .035), and higher transitivity (Trans, P = .033) in CRT animals compared to Sham (Fig. 5D). Irradiation also affected regional connectivity, in which multiple regions were hypo-connected in CRT compared to Sham (P = .004), familywise error corrected. Regional connection statistics can be found in Supplementary Material.

White Matter

White matter, gray matter, and cerebral spinal fluid segmentation using T_1-weighted, T_2-weighted, and proton density images showed a trend toward decrease in white matter at 12 months after CRT (Supplementary Figure 6). Percent white matter and cerebrospinal fluid were not significantly different between CRT and Sham brains. However, gray matter was significantly lower in CRT brains (P = .004). This reduction in gray matter matches our observed reduction in volume of brain regions that were predominantly composed of gray matter (Supplementary Table 4).

Imaging Feature and Cognitive Performance Correlation

Imaging markers from DTI were highly correlated with percent accuracy at Stage 7. Cognitive metrics averaged over the 5 days of testing at Stage 7 showed there was a high

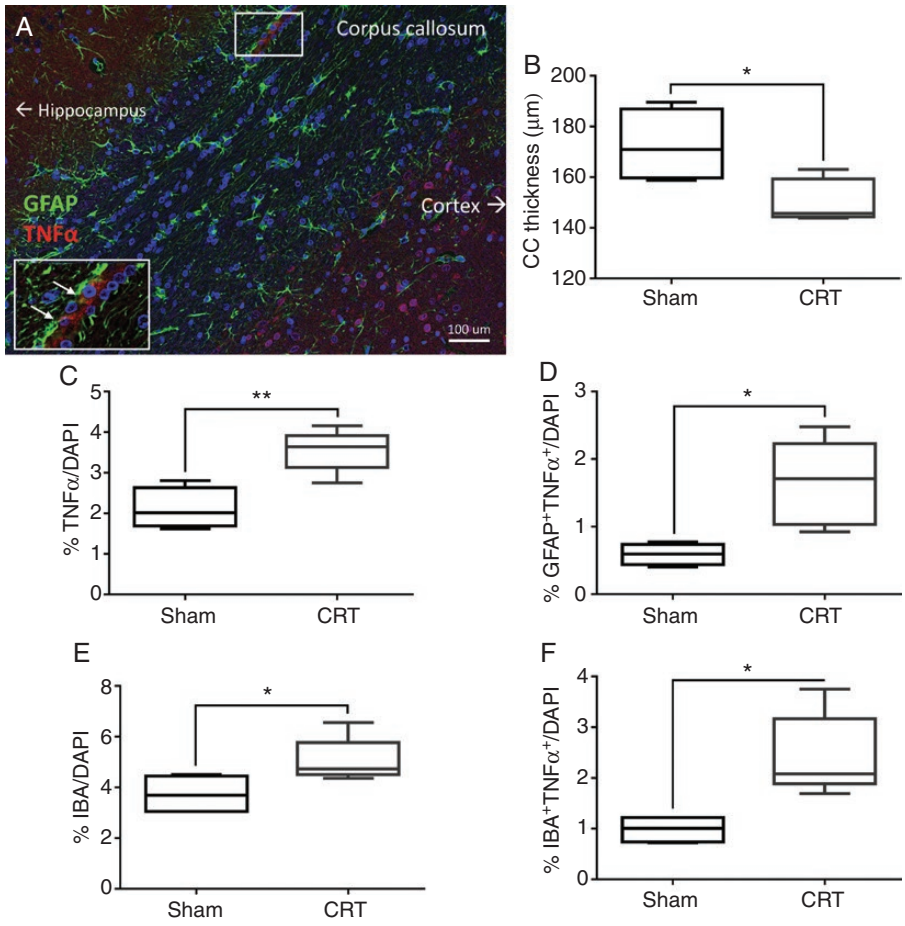

Fig. 3. Neuroinflammation and demyelination observed at 12 months after cranial radiotherapy (CRT). (**A**) CRT brain sections immunostained for markers of inflammation; TNFα (tumor necrosis factor alpha, red) and GFAP (glial fibrillary acidic protein, green). (**B**) Reduction in corpus callosum (CC) thickness after CRT as visualized using myelin basic protein (MBP) staining. (**C** and **D**) An increase in TNFα+ and GFAP+ cells was found following CRT versus Sham. (**E** and **F**) Quantification of activated microglia (IBA-1 and TNFα) showed increase in CRT brains. *$P \leq .05$, **$P \leq .01$.

correlation of accuracy to Trans ($P = .020$), Mod ($P = .035$), Gamma ($P = .032$), Sigma ($P = .030$), Fiber number ($P = .036$) and FA value ($P = .013$) (Fig. 6). However, the other cognitive metrics, percent correct, omissions, and premature responses did not correlate with any of the MR measurements.

Discussion

In this study, we have used our preclinical model of radiation-induced brain injury to identify late-term imaging changes using MR and PET imaging. We first verified that our CRT rats have cognitive deficits by testing their executive function. To our knowledge, this is one of the few studies looking at early and late-term effect of CRT on executive function in rodent models. During training, Sham animals on average reached a higher stage compared to CRT. CRT animals also spent significantly more days in Stage 5, compared to Sham animals, before passing the stage. Furthermore, immunohistochemistry revealed clear signs of late-term neuroinflammation, with CRT brains having significantly increased TNFα positive cells coupled with increased numbers of microglia. DTI analysis revealed regional volumetric changes and functional changes which includes reduction in FA value, fiber number, and reorganization of the brain's connectivity in CRT animals. ^{18}F-FDG-PET imaging showed an increase in glucose uptake in the brain of CRT animals. Finally, cognitive measures were found to be significantly correlated with six imaging features.

The differential in volumetric changes between brain regions demonstrates the heterogeneous response of the brain to CRT and highlights the fact that some regions are more radioresistant/radiosensitive than others. However, these volumetric changes were not always indicative of functional changes as only two brain regions, corpus callosum and striatum, showed changes in both volume and FA values. Therefore, volumetric changes alone may not be informative of cognitive outcome. FA values have been established as a sensitive measure of radiation-induced brain injury, specifically in changes within white matter.[13]

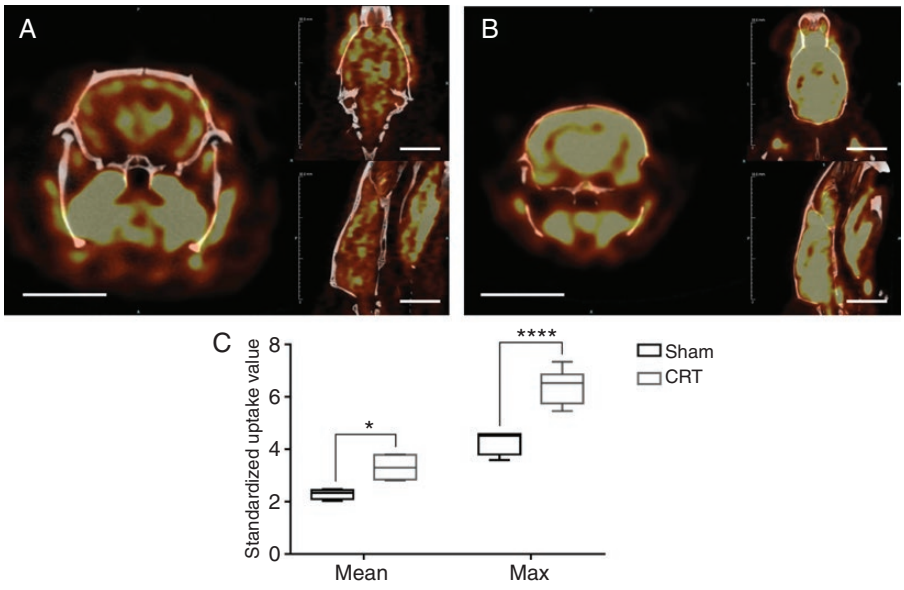

Fig. 4. PET imaging at 12 months after cranial radiotherapy (CRT) demonstrate changes in metabolic activity in the brain. Metabolic imaging of (**A**) Sham animal and (**B**) CRT animals with ^{18}F-FDG-PET. A heat map of glucose uptake is shown where the color yellow indicates higher uptake. (**C**) Glucose uptake was quantified using standardized uptake value (SUV) of the entire brain volume. Mean and Max SUV was higher in CRT brains than Sham. Scale bar = 10 mm, *$P \leq .05$, ****$P \leq .0001$.

Similar to previous studies, we also observed decreased FA values in whole brain and specific regions including the hippocampus.[12,38–40] These changes can be correlated to cognitive performance as demonstrated by Mabbot et al.[11] and Khong et al.,[41] in which decreased FA values were indicative of decreased cognitive performance. Using the 5-CSRTT cognitive test we also observed a similar correlation with accuracy. We further identified the number of fibers to be highly correlated to cognitive performance. Even though white matter damage was observed using the FA value we did not find the percent white matter to be indicative of CRT-induced injury or cognitive performance in our preclinical model. However, Reddick et al. found that medulloblastoma patients treated with CRT developed less normal appearing white matter and that reductions in white matter volume in the frontal lobes were associated with decreased cognitive performance in executive function.[42,43] This discrepancy may be due to the relative preponderance of white matter in humans or possibly our choice of animal model and radiation regimen.

Using connectome analysis, trajectory of white matter fibers obtained from DTI we identified fiber track changes, including local and global changes to the brain network's connectivity and organization. CRT animals had higher transitivity and lower global efficiency, indicating increases in segregated networks and longer path lengths between these segregated areas.[33] CRT appears to have caused a reorganization of the brain network resulting in greater specialization at the expense of network integration. Lower integration was also reflected in the significantly lower regional connectivity associated with CRT. Similar to our results, Bahrami et al.[44] also measured a significant increase in transitivity after radiotherapy but contrary to us they observed a significant increase in global efficiency. Discrepancies between these two findings may be attributed to the fact that their study was done in adult brain tumor patients, whereas ours was in a preclinical pediatric rat model that did not include tumor presence and hence no surgery and/or chemotherapy. Our results agree with previous results from our lab, Sahnoune et al.,[25] even though we used a different animal strain and radiation regime, indicating that global efficiency may be a marker of radiation damage that is independent of radiation dose. In addition to characterization of the global brain network, these metrics can also be used to gauge cognitive performance in an objective manner. The identified features that included Transitivity, Modularity, Normalized cluster coefficient (Gamma), Small Worldness Index (Sigma), fiber number and FA value in this preclinical model are potential new imaging markers for assessing patient response to radiotherapy and tracking the progression of CRT-induced brain injury in a noninvasive manner.

Neuroinflammation has been implicated as a driving force in radiation-induced brain injury. CRT induces an inflammatory response with increases in TNFα, microglia, and astrocyte activation.[5,45] This inflammatory response can persist up to months after CRT as shown in preclinical models.[46] The activation of these brain immune cells could contribute to the increased glucose metabolism we observed. To our knowledge this is the first report on the use of ^{18}FDG-PET to image late-term CRT-induced global increase in brain metabolic activity. Previous studies have used this imaging technique to diagnose and identify neurodegenerative disease such as Alzheimer and Parkinson's.[47] Krull et al.[48] also observed late-term metabolic changes in acute lymphoblastic leukemia patients however the

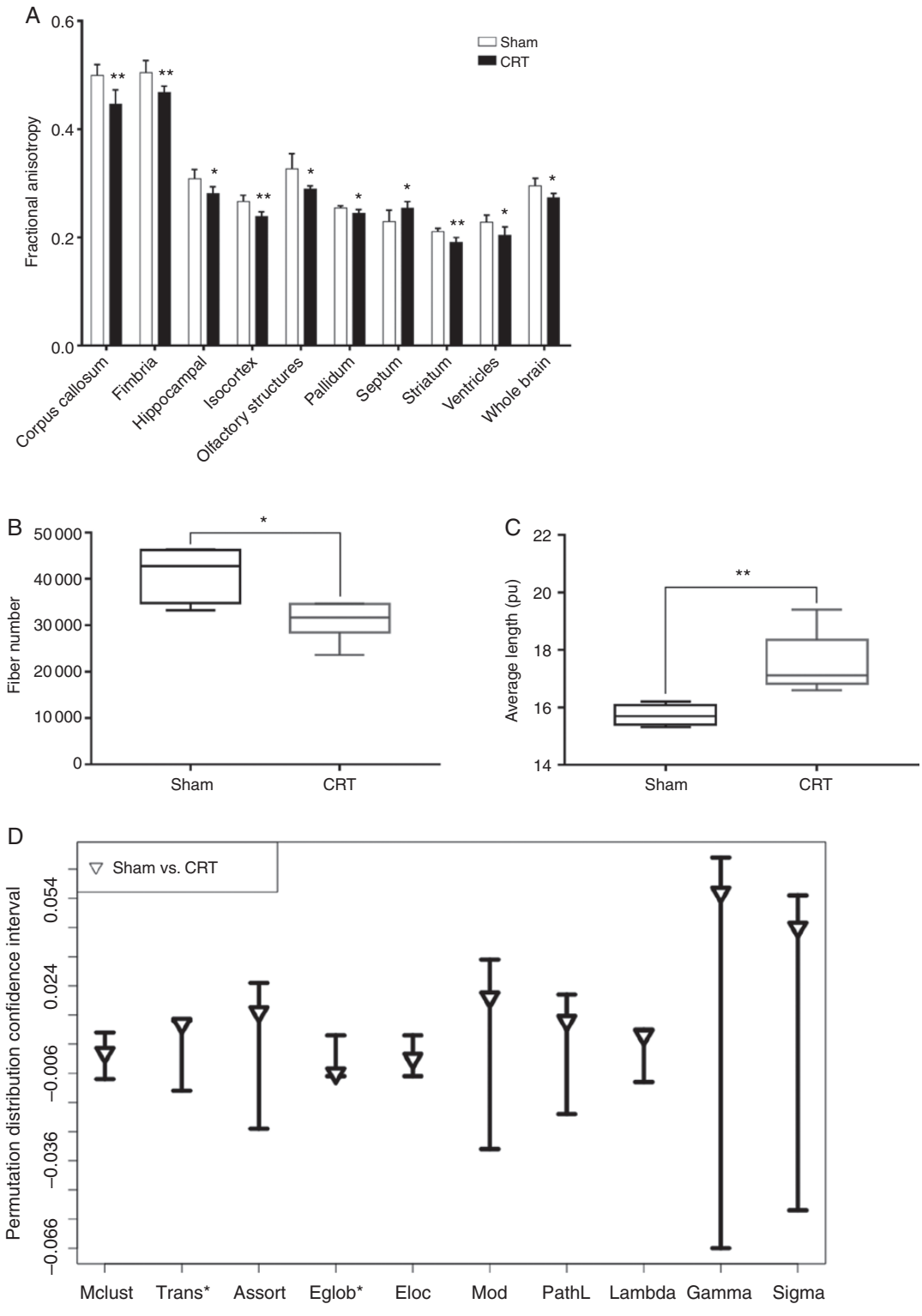

Fig. 5. Diffusion tensor imaging reveals changes in brain regions fractional anisotropy (FA), fiber values, and neuronal organization at 12 months after cranial radiotherapy (CRT). (**A**) FA values in significantly different brain regions as measured in Sham and irradiated animals. 38% of brain regions analyzed showed significant changes after CRT. (**B**) Overall whole brain fiber number was reduced in CRT animals. (**C**) Whole brain average fiber length increased after CRT. (**D**) Global connectomes affected after CRT. Data are shown as 95% permutation distribution confidence interval with triangle indicating the mean difference $^{*}P \leq .05$ from permutation testing. Mclust = Model Based Clustering, Trans = Transitivity, Assort = Assortativity, Eglob = Global Efficiency, Eloc = Local Efficiency, Mod = Modularity, and PathL = Path Length. $^{*}P \leq .05$, $^{**}P \leq .01$.

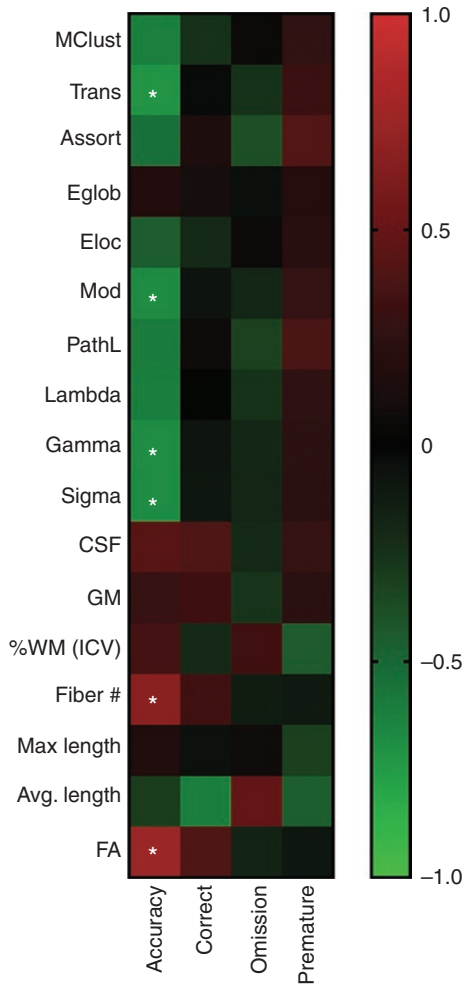

Fig. 6. Correlation matrix of image features and five-choice serial reaction time task (5-CSRTT) performance. Image features derived from diffusion tensor imaging and white matter analysis were correlated to cognitive metrics as measured at Stage 7 by 5-CSRTT, at 12 months after cranial radiotherapy. Significant Pearson's correlation is marked by asterisks. Mclust = Model Based Clustering, Trans = Transitivity, Assort = Assortativity, Eglob = Global Efficiency, Eloc = Local Efficiency, Mod = Modularity, PathL = Path Length, CSF = cranial spinal fluid, GM = gray matter, %WM = % white matter (intercranial volume), FA = fractional anisotropy.

treatment plan also included chemotherapy. Interestingly, the increase in metabolism was observed throughout the brain, even in regions such as the olfactory bulb and cerebellum that may have been partially shielded during irradiation, which seems to indicate that neuroinflammation is systemic and not localized to exposed tissue. It should also be noted that the reorganization of the brain network measured by our functional imaging could be responsible, either together with neuroinflammation or solely, for the increase in glucose uptake in the irradiated brains compared to their age matched controls. Even though further work is still needed to identify the underlying driver of the observed ^{18}FDG-PET signal, the information from the images can still provide an additional tool for longitudinal surveillance and insight into how these metabolic changes may affect cognitive performance.

A strength of this study is in our use of pediatric rats to mimic stage of brain development of children receiving CRT. However, this is a complex study that includes animal cognition and noninvasive translational imaging techniques and therefore has several limitations including imaging sample size, the *ex vivo* technique used to acquire DTI data and the use of only male animals. Owing to the shortened life span of our preclinical model and the consequent limitation on the pediatric period this study used a hypofraction regiment to ensure animals are still considered pediatric by the end of the treatment period. We have also limited our study to the 5-CSRTT, a frontal lobe executive function task; however, the inclusion of similar cognitive tests could potentially uncover new imaging-cognition correlations. However, this 5-CSRTT cognitive test requires several weeks of training (~7 wk) for both CRT and Sham groups which results in considerable enrichment of cognitive performance which limited testing to after CRT. Although this is accounted for in the comparison between these groups nevertheless it might have lessened the severity of damage observed in our studies. Despite these limitations, we have identified several highly correlative imaging markers of late-term radiation-induced cognitive deficits

Conclusion

Although there are currently no functional markers that can identify individuals susceptible to radiation-induced brain injury and the resulting cognitive impairment, medical images may be a valuable tool. In this study, we established a rodent model which exhibit long-term executive function impairment after CRT, mimicking some of the radiation-induced cognitive impairments often observed in the clinic. In addition, we also identified several imaging markers of late-term CRT-induced damage using MR structural and functional imaging that are highly correlated to cognitive performance. These imaging markers, derived from scans that are commonly acquired in the standard clinical workflow, could potentially provide clinicians with a noninvasive tool to help detect the severity of CRT treatment side effects on a patient-to-patient basis. Future work will investigate if these imaging markers at earlier time points could provide a tool for risk assessment of radiation-induced cognitive impairment.

Supplementary Material

Supplementary material is available at *Neuro-Oncology Advances* online.

Keywords

brain | cognition | connectome | imaging | radiation.

Funding

This work was supported in part by a grant from Cancer Prevention Research Institute of Texas (CPRIT) [RP130573CPRIT to M.W.G.]; SBIR Phase II Topic 291 [contract no. HHSN261201300076C to D.H.C.]; and National Cancer Institute [1R01CA208535 to D.R.G.].

Acknowledgments

The authors would like to thank Texas Children's Hospital for use of the Small Animal Imaging Facility. The authors would also like to thank David Flint for his assistance in editing the manuscript.

Conflict of interest statement. The authors have declared that no conflict of interest exists.

Authorship statement: Tien T. Tang and Janice A. Zawaski wrote the manuscript and all authors contributed to editing. Tien T. Tang, Janice A. Zawaski, and M. Waleed Gaber designed research study. Tien T. Tang, Janice A. Zawaski, and Christine A. Beamish acquired data. Tien T. Tang, Janice A. Zawaski, Shelli R. Kesler, Christine A. Beamish, Wilburn E. Reddick, and John O. Glass analyzed data. Darrell H. Carney, Omaima M. Sabek, and M. Waleed Gaber provided funding sources.

References

1. Ullrich NJ, Embry L. Neurocognitive dysfunction in survivors of childhood brain tumors. *Semin Pediatr Neurol.* 2012;19(1):35–42.
2. Gajjar AJ, Robinson GW. Medulloblastoma-translating discoveries from the bench to the bedside. *Nat Rev Clin Oncol.* 2014;11(12):714–722.
3. Wilson CM, Gaber MW, Sabek OM, Zawaski JA, and Merchant TE. Radiation-induced astrogliosis and blood-brain barrier damage can be abrogated using anti-TNF treatment. *Int. J. Radiation Oncology Biol. Phys.* 2009;74(3):934–41.
4. Schultheiss TE, Stephens LC. Invited review: permanent radiation myelopathy. *Br J Radiol.* 1992;65(777):737–753.
5. Tofilon PJ, Fike JR. The radioresponse of the central nervous system: a dynamic process. *Radiat Res.* 2000;153(4):357–370.
6. Brinkman TM, Reddick WE, Luxton J, et al. Cerebral white matter integrity and executive function in adult survivors of childhood medulloblastoma. *Neuro Oncol.* 2012; 14 (suppl 4):iv25–36.
7. Rodgers SP, Zawaski JA, Sahnoune I, Leasure JL, Gaber MW. Radiation-induced growth retardation and microstructural and metabolite abnormalities in the hippocampus. *Neural Plast.* 2016;2016:3259621.
8. Lumniczky K, Szatmári T, Sáfrány G. Ionizing radiation-induced immune and inflammatory reactions in the brain. *Front Immunol.* 2017;8:517.
9. Schatz J, Kramer JH, Ablin A, Matthay KK. Processing speed, working memory, and IQ: a developmental model of cognitive deficits following cranial radiation therapy. *Neuropsychology.* 2000;14(2):189–200.
10. Dellani PR, Eder S, Gawehn J, et al. Late structural alterations of cerebral white matter in long-term survivors of childhood leukemia. *J Magn Reson Imaging.* 2008;27(6):1250–1255.
11. Mabbott DJ, Noseworthy MD, Bouffet E, Rockel C, Laughlin S. Diffusion tensor imaging of white matter after cranial radiation in children for medulloblastoma: correlation with IQ. *Neuro Oncol.* 2006;8(3):244–252.
12. Khong PL, Kwong DL, Chan GC, Sham JS, Chan FL, Ooi GC. Diffusion-tensor imaging for the detection and quantification of treatment-induced white matter injury in children with medulloblastoma: a pilot study. *AJNR Am J Neuroradiol.* 2003;24(4):734–740.
13. Alexander AL, Lee JE, Lazar M, Field AS. Diffusion tensor imaging of the brain. *Neurotherapeutics.* 2007;4(3):316–329.
14. Bullmore E, Sporns O. Complex brain networks: graph theoretical analysis of structural and functional systems. *Nat Rev Neurosci.* 2009;10(3):186–198.
15. Wahl RL, Quint LE, Greenough RL, Meyer CR, White RI, Orringer MB. Staging of mediastinal non-small cell lung cancer with FDG PET, CT, and fusion images: preliminary prospective evaluation. *Radiology.* 1994;191(2):371–377.
16. Kelloff GJ, Hoffman JM, Johnson B, et al. Progress and promise of FDG-PET imaging for cancer patient management and oncologic drug development. *Clin Cancer Res.* 2005;11(8):2785–2808.
17. Phelps ME, Huang SC, Hoffman EJ, Selin C, Sokoloff L, Kuhl DE. Tomographic measurement of local cerebral glucose metabolic rate in humans with (F-18)2-fluoro-2-deoxy-D-glucose: validation of method. *Ann Neurol.* 1979;6(5):371–388.
18. van Waarde A, Cobben DC, Suurmeijer AJ, et al. Selectivity of 18F-FLT and 18F-FDG for differentiating tumor from inflammation in a rodent model. *J Nucl Med.* 2004;45(4):695–700.
19. Love C, Tomas MB, Tronco GG, Palestro CJ. FDG PET of infection and inflammation. *Radiographics.* 2005;25(5):1357–1368.
20. Kubota R, Yamada S, Kubota K, Ishiwata K, Tamahashi N, Ido T. Intratumoral distribution of fluorine-18-fluorodeoxyglucose in vivo: high accumulation in macrophages and granulation tissues studied by microautoradiography. *J Nucl Med.* 1992;33(11):1972–1980.
21. Sahakian BJ, Owen AM, Morant NJ, et al. Further analysis of the cognitive effects of tetrahydroaminoacridine (THA) in alzheimer's disease: assessment of attentional and mnemonic function using CANTAB. *Psychopharmacology (berl).* 1993;110(4):395–401.
22. Bari A, Dalley JW, Robbins TW. The application of the 5-choice serial reaction time task for the assessment of visual attentional processes and impulse control in rats. *Nat protoc.* 2008;3(5):759–767.
23. Reddick WE, Glass JO, Cook EN, Elkin TD, Deaton RJ. Automated segmentation and classification of multispectral magnetic resonance images of brain using artificial neural networks. *IEEE Trans Med Imaging.* 1997;16(6):911–918.
24. Tyszka JM, Readhead C, Bearer EL, Pautler RG, Jacobs RE. Statistical diffusion tensor histology reveals regional dysmyelination effects in the shiverer mouse mutant. *Neuroimage.* 2006;29(4):1058–1065.
25. Sahnoune I, Inoue T, Kesler SR, et al. Exercise ameliorates neurocognitive impairments in a translational model of pediatric radiotherapy. *Neuro Oncol.* 2018;20(5):695–704.
26. Mori S, Zhang J. Principles of diffusion tensor imaging and its applications to basic neuroscience research. *Neuron.* 2006;51(5):527–539.
27. Jiang H, van Zijl PC, Kim J, Pearlson GD, Mori S. Dtistudio: resource program for diffusion tensor computation and fiber bundle tracking. *Comput Methods Programs Biomed.* 2006;81(2):106–116.
28. Calabrese E, Badea A, Watson C, Johnson GA. A quantitative magnetic resonance histology atlas of postnatal rat brain development with regional estimates of growth and variability. *Neuroimage.* 2013;71:196–206.

29. Zhang W, Li X, Zhang J, et al. Landmark-referenced voxel-based analysis of diffusion tensor images of the brainstem white matter tracts: application in patients with middle cerebral artery stroke. *Neuroimage.* 2009;44(3):906–913.
30. Woods RP, Grafton ST, Holmes CJ, Cherry SR, Mazziotta JC. Automated image registration: I. General methods and intrasubject, intramodality validation. *J Comput Assist Tomogr.* 1998;22(1):139–152.
31. Woods RP, Grafton ST, Watson JD, Sicotte NL, Mazziotta JC. Automated image registration: II. Intersubject validation of linear and nonlinear models. *J Comput Assist Tomogr.* 1998;22(1):153–165.
32. Ceritoglu C, Oishi K, Li X, et al. Multi-contrast large deformation diffeomorphic metric mapping for diffusion tensor imaging. *Neuroimage.* 2009;47(2):618–627.
33. Rubinov M, Sporns O. Complex network measures of brain connectivity: uses and interpretations. *Neuroimage.* 2010;52(3):1059–1069.
34. Sporns O, Betzel RF. Modular brain networks. *Annu Rev Psychol.* 2016;67:613–640.
35. Bassett DS, Bullmore E. Small-world brain networks. *Neuroscientist.* 2006;12(6):512–523.
36. Zalesky A, Fornito A, Bullmore E. On the use of correlation as a measure of network connectivity. *Neuroimage.* 2012;60(4):2096–2106.
37. Zalesky A, Fornito A, Bullmore ET. Network-based statistic: identifying differences in brain networks. *Neuroimage.* 2010;53(4):1197–1207.
38. Qiu D, Leung LH, Kwong DL, Chan GC, Khong PL. Mapping radiation dose distribution on the fractional anisotropy map: applications in the assessment of treatment-induced white matter injury. *Neuroimage.* 2006;31(1):109–115.
39. Qiu D, Kwong DL, Chan GC, Leung LH, Khong PL. Diffusion tensor magnetic resonance imaging finding of discrepant fractional anisotropy between the frontal and parietal lobes after whole-brain irradiation in childhood medulloblastoma survivors: reflection of regional white matter radiosensitivity? *Int J Radiat Oncol Biol Phys.* 2007;69(3):846–851.
40. Connor M, Karunamuni R, McDonald C, et al. Regional susceptibility to dose-dependent white matter damage after brain radiotherapy. *Radiother Oncol.* 2017;123(2):209–217.
41. Khong PL, Leung LH, Fung AS, et al. White matter anisotropy in post-treatment childhood cancer survivors: preliminary evidence of association with neurocognitive function. *J Clin Oncol.* 2006;24(6):884–890.
42. Reddick WE, Glass JO, Palmer SL, et al. Atypical white matter volume development in children following craniospinal irradiation. *Neuro Oncol.* 2005;7(1):12–19.
43. Glass JO, Ogg RJ, Hyun JW, et al. Disrupted development and integrity of frontal white matter in patients treated for pediatric medulloblastoma. *Neuro Oncol.* 2017;19(10):1408–1418.
44. Bahrami N, Seibert TM, Karunamuni R, et al. Altered network topology in patients with primary brain tumors after fractionated radiotherapy. *Brain Connect.* 2017;7(5):299–308.
45. Hong JH, Chiang CS, Campbell IL, Sun JR, Withers HR, McBride WH. Induction of acute phase gene expression by brain irradiation. *Int J Radiat Oncol Biol Phys.* 1995;33(3):619–626.
46. Chiang CS, Hong JH, Stalder A, Sun JR, Withers HR, McBride WH. Delayed molecular responses to brain irradiation. *Int J Radiat Biol.* 1997;72(1):45–53.
47. Mosconi L, Tsui WH, Herholz K, et al. Multicenter standardized 18F-FDG PET diagnosis of mild cognitive impairment, alzheimer's disease, and other dementias. *J Nucl Med.* 2008;49(3):390–398.
48. Krull KR, Minoshima S, Edelmann M, et al. Regional brain glucose metabolism and neurocognitive function in adult survivors of childhood cancer treated with cranial radiation. *J Nucl Med.* 2014;55(11):1805–1810.